Current Chemistry Letters 12 (2023) 459–470

Contents lists available atGrowingScience

Current Chemistry Letters

homepage: www.GrowingScience.com

An experimental investigation on metallurgical and corrosion behavior of atmospheric plasma sprayed Stellite 6 powder on AISI 304 stainless steel

Sangita Sarangi[a*], Ajit Kumar Mishra[a] and Seshadev Sahoo[a]

[a]*Department of Mechanical Engineering, Institute of Technical Education and Research, Siksha O Anusandhan (Deemed to be University), Bhubaneswar, Odisha, India-751030*

C H R O N I C L E

Article history:
Received May 23, 2022
Received in revised form
June 25, 2022
Accepted October 21, 2022
Available online
October 21, 2022

Keywords:
Stellite 6 Coating
Microstructure
Microhardness
Plasma spray
XRD

A B S T R A C T

An experimental investigation was undertaken to study the Cobalt-based Stellite 6, powder deposited on SS 304 stainless steel substrate without any intermittent layer using an atmospheric plasma spray deposition process by varying the thickness of coating in the range of 74 µm, 128 µm, and 215 µm. The effect of coating thickness on metallurgical properties and corrosion resistance behavior was investigated. Optical microscopy, Scanning Electron Microscopy (SEM), and Energy Dispersive X-ray Spectroscopy (EDS) were employed to study the morphology of Stellite 6 coating. X-Ray Diffraction was used for structural analysis and to identify the phase formation. It was observed that the sample with 128 µm coating thickness provides the best result concerning microhardness and microstructure characteristics whereas the sample with 215 µm coating thickness provides the best corrosion resistance property. The reasons for the deviation were investigated and the factors responsible for the deviation were assigned in this investigation.

1. Introduction

It cannot be denied that applied science plays an important role in the functioning of our life. Nowadays the government is giving a lot of emphasis to protect the environment by harnessing green energy and adopting renewable energy resources. Incentives are given to utilize non-conventional methods to generate electricity such as solar, tidal, and wind energy. Wind turbines are placed onshore or offshore to harness wind energy. In this connection, very large structures are being erected near the shore or inside the sea to harness the wind energy for potential power generation. These structures are operated in a hostile corrosive atmosphere demanding a superior material for corrosion inhibition.

AISI 304 is a structural grade stainless steel and is more frequently used in chemical, and power plant industries because of its superior corrosion-resistant properties, but its relatively low hardness and wear resistance property limits its applications in various sectors.[1] This steel can be coated with a protected layer to improve further the corrosion resistance characteristics and accentuate an improvement of the life of the components. Hence, a large number of surface coating procedures are adopted on this Stainless-steel material to improve its mechanical properties as well as the working life of these components. Surface coating is one of the best solutions to reduce corrosion, especially products like hydro turbine blades, exhaust valves in engines, cutting tools, molds, dies, etc. which are functioning in a hostile environment.[2-4]

Different types of surface coating procedures such as Plasma Transferred Arc deposition process (PTA), Gas Tungsten Arc Welding Process (GTAW), High-Velocity Oxygen Fuel (HVOF) spraying, and Cold gas spraying are adopted for coating the surface subjected to wear and corrosion, resulting in an improvement in the reliability of such components.

* Corresponding author.
E-mail address sangitasarangi282@gmail.com (S. Sarangi)

doi: 10.5267/j.ccl.2022.10.003

Atmospheric plasma spray is also a type of surface coating technique that uses various types of coating powders like ceramic, metallic, polymeric, composite, etc. for coating any kind of materials.[5] The coating produced by the plasma spray technique has resulted in better corrosion resistance with improving the service life of the substrate materials. In this process, the coating powder is initiated into the thermal plasma jet which gets melted and moved toward the substrate at a very faster rate. These molten droplets are quenched after impact with the substrate forming a layered microstructure and may also contain very few defects like pores, splats, and micro cracks. Also, coatings of good quality, and adherence with higher deposition efficiency are provided by the plasma spraying technique.[6, 7] Plasma-sprayed coatings are applied to several industrial items.[8, 9] They can improve surface characteristics such as thermal and wear resistance, chemical stability, and corrosion resistance, as well as certain mechanical and electrical characteristics that are crucial for usage in harsh environments. The mechanical properties of NiTi shape-memory alloy coatings, including hardness (Vickers' microhardness), adhesion strength (ASTMC-633) and wear resistance (solid particle erosion), were examined after they were deposited by atmospheric plasma spray (APS) on mild steel substrates.[10]

A large number of coating materials are available for their application on different types of surfaces to improve the mechanical and metallurgical properties of the materials.[11, 12] Stellite 6 is a Cobalt-based super-alloy product broadly used for coating with improved corrosion-resistant properties and operating at an elevated temperature up to 1095ºC.[13, 14] The presence of Chromium in Stellite 6 also imparts added strength and improves the corrosion and oxidation resistance properties of the alloy by forming carbides of type Cr_7C_3 and $Cr_{23}C_6$. Stellite 6, thus having excellent corrosion-resistant characteristics, is identified for coating on AISI 304-grade stainless steel.

Budzynski et al.[15] investigated the tribological behavior of Stellite 6 alloy with ion implantation. This incomprehensive study mostly focused on the effect of nitrogen ion implantation to change the properties of the Stellite 6 alloy. Thawari et al.[16] produced a wear-resistant Stellite 6 coating with the crack-free layer in the laser cladding method and investigated the mechanical and microstructural properties by adding a buffer layer. The authors found that Stellite coating with a buffer layer has shown promising results as compared to without a buffer layer.

The mechanical, microstructural, and tribological properties of Stellite coated Stainless steel was investigated by Jeyaprakash et al.[17] From this investigation, the authors observed that Stellite 6 coating has shown a dendritic structure due to rapid cooling which increases the hardness of the coatings. The effects of process parameters on mechanical and tribological properties of Stellite-6 coatings obtained by Cold Gas Dynamic Spray and High-Velocity Oxy-Fuel Spray were investigated by Magaro et al.[18] and Sassatelli et al.[19] The authors have optimized the coating thickness concerning the mechanical properties like hardness and Young's modulus of Stellite 6 material adopting cold gas dynamic spray and HVOF process and also studied the microstructural and mechanical properties. The changes in microstructure, microhardness, and corrosion resistance of laser cladded Stellite-6 and tungsten carbide metal matrix composites coated on AISI S355 steel were compared and analyzed.[20]

Previous studies indicate a large number of physical and chemical processes are available to increase the hardness of the surfaces to enhance wear-resistant and corrosion properties.[2, 3, 18, 19] However, there was a lacking a systematic approach to investigate the mechanical and metallurgical behavior of Stellite 6 coating on AISI 304 Stainless Steel by the atmospheric plasma spray process. Also, the combination of coating thickness coupled with microhardness, corrosion resistance property, and microstructure of the material was less investigated. In the present study, efforts have been made to coat the AISI 304 Stainless Steel substrate with Stellite 6 powder using the atmospheric plasma spray technique by varying the coating thickness and investigating the structural, functional, and mechanical properties. The effect of various coating thicknesses on their mechanical and functional behavior along with morphological characteristics is investigated for optimizing the benefits of coating.

2. Results and Discussion

2.1. Characterization of Stellite 6 powder

The commercially procured Stellite 6 powder is characterized by Scanning electron microscopy (SEM) and the morphology of the powder is shown in **Fig. 1 (a)**. The micrograph shows that most of the particles are spherical with regular shapes with little agglomeration seen for smaller-size particles. Agglomeration of particles sometimes takes place leading to a variation in shape. Moreover, very few fragmented particles also exist. Therefore, with the presence of regular shape particles, the coating produced by Stellite 6 powder is generally smooth and homogenous. **Fig. 1 (b)** shows the particle size distribution and the size concentration. It is found that the size range of particles lies between 34 μm to 18 μm. It has a peak value of 25 μm with a Gaussian distribution of 8.18. This value indicates around 25μm is the film thickness that will be obtained in a single pass at the time of coating. The X-Ray Diffraction pattern of Stellite 6 powder is shown in **Fig. 1 (c).** It is evident from the diffraction pattern that the powder consists of a Co-based solid solution with prominent peaks with a diffraction angle of 43 degree. It has very low peaks with uniform distributions of prominently Cr_7C_3 carbide phase. Cobalt possesses a hexagonal close-pack structure at room temperature.[21]

The Stellite 6 powder is normally produced by spray drying and the atomization process. During the atomization process, a high cooling rate is experienced, due to which a low amount of Cr_7C_3 carbide is observed. This finding is also corroborated.[22]

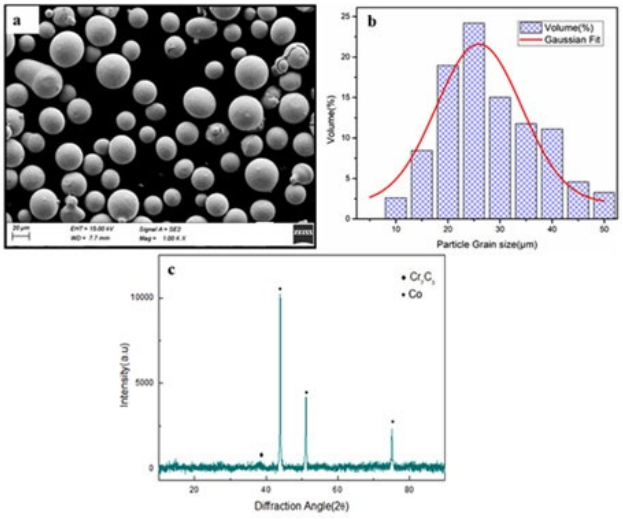

Fig. 1. (a) SEM micrograph of Stellite 6 powder, (b) Particle size distribution, and (c) XRD plot of Stellite 6 powder

2.2 Calculation of Coating thickness and Adhesion Strength

Coating of Stellite 6 powder on the vertically held steel substrate is carried out in a layered approach through passes with longitudinal and transverse direction and a 25 μm thickness of the coating is obtained in every pass. An optical micrograph image of the substrate-coating interface of the plasma-spray coated Stellite 6 on AISI 304 Stainless steel substrate and also a clear image (SEM) of coating is shown in **Fig. 2.** From the micrograph of **Figs. 2(a), (b),** and **(c)** three distinct layers are observed. The first layer (marked 1) is the bottom layer depicts SS 304 steel substrate, the intermittent layer (marked 2) represents the coated surface, and the top layer (marked 3) is the resin. The above figures indicate that the deposition of Stellite 6 powder coating is present in a lamellar texture parallel to the steel surface. It is found that sample 3 depicts the most uniform coating thickness whereas sample 1 has an irregular coating thickness as compared with all three micrographs." Average coating thickness as measured from the micrographs is 74 μm, 128 μm, and 215 μm for 1st, 2nd, and 3rd samples respectively and the variation in coating thickness ranges between 38.43%, 20.23%, and 7.69% respectively. It can be inferred that without changing the process parameters for atmospheric plasma spray deposition technology, larger coated products exhibit a sound and smooth coating. Large particles associated with the powders are melted instantly, incur rapid solidification, and get deposited uniformly in the wall of the substrate. This phenomenon could not be witnessed while depositing the coating material on the lower coating thickness products. Some unmelted particles in the form of splats and partially melted particles in the form of pores were observed in **Fig. 2(d)** which is the characteristic feature of plasma spray coatings. These pores or voids which are marked from SEM are black.

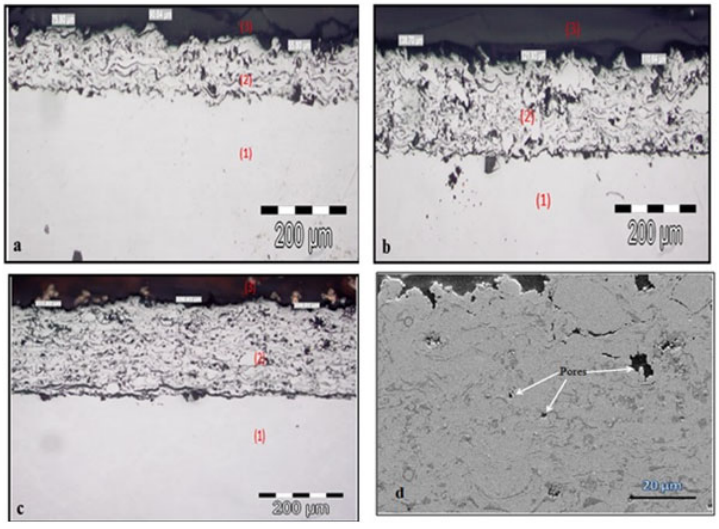

Fig. 2. Substrate-Coating Interface shown by Optical Micrograph of the as-coated Stellite 6 on Stainless Steel substrate" (a) for sample 1, (b) for sample 2, (c) for sample 3 (1= substrate, 2= Stellite 6 coating, 3=resin) and (d) magnified image of coating(SEM)

The separation of the coating has taken place at the interface of the coating and substrate which is shown in Fig. 3. In all three samples, adhesion pull-up strength has a magnitude varying between 26.5± 2MPa corresponding to strong intra-bonding in Stellite 6 particles. Also, after examining disjoined study surfaces, it is observed that a negligible amount of coated material has been pulled out from the coating. In the case of sample 3 having 215µm coatings thickness, the adhesion strength value is beyond 28 MPa, showing an appreciable amount of visible coating pull-out. The strength obtained in adhesion testing is considered good because of a greater number of touch points between the well-flattened splats. The more touch points indicate the stud is having more surface area of contact. It means the contact surface area is increased and a higher amount of force is required to separate the coated material from the substrate.

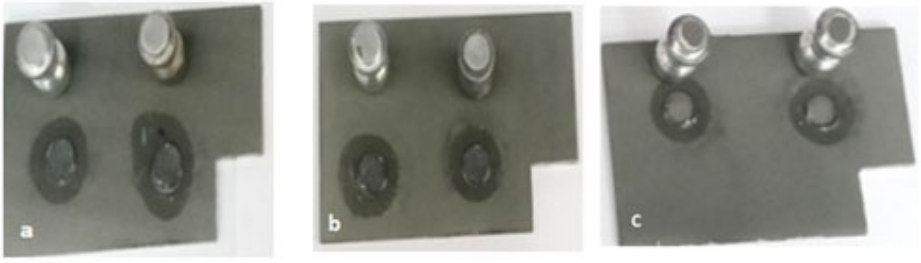

Fig. 3. Adhesion tested Samples (a) Sample 1 (b) Sample 2 (c) Sample 3

2.3 Density, Porosity, and Surface Roughness of Stellite 6 coating

The coating density is calculated by peeling a small portion from the surface of the substrate by mechanical means. Archimedes's principle [23] as shown in Eq. (1) is used for the determination of density.

$$\textit{Density of the coating} = (d_w \times M_a) / (M_a - M_w) \quad (1)$$

where d_w is the density of water, M_a is the weight of the coated sample in the air (gm), M_w is the weight of the coated sample in water (gm). Material with higher coating density indicates a superior and homogeneous coating justifying a superior load requirement for its delamination and removal leading to failure. Physical parameters such as density, porosity, and surface roughness are depicted in **Table 1**. The density of Stellite 6 is reported as 8.69 g/cm^3. [24] The calculated value of the density of the coating was 8.44 g/cm^3. Optical microscopic image analysis (OMIA) techniques were used for the determination of the homogeneity of the coating. The porosity of coated samples was calculated by Image J public free domain software.[25] Ten different observations are taken at different locations and the porosity of the coated surface is calculated using the statistical average method. The porosity value for the plasma sprayed coating is found to be in the range of 2.9 ± 0.05%. Sidhu et al.[26] observed the porosity of plasma-sprayed Stellite 6 coating lies between 2-3.5%. From the table, it is observed that sample 2 has the lowest porosity value.

The surface roughness of the coated product was measured using a surface roughness instrument. Five roughness readings are taken on each sample and their average value is taken as the surface roughness. The coated product surface roughness value for all the samples is measured using a surface roughness meter and its roughness values vary between 4.8 ± 0.02 µm whereas with the adoption of the HVOF process the value obtained is 4.892 ± 0.38 µm. This indicates a close tolerance in the surface roughness for the atmospheric plasma spray technique is obtained as compared to the HVOF process where a wide variation was observed.[27]

Table 1. Density, porosity, and surface roughness of the Stellite 6 coated samples

Samples	Coating thickness	Density	Porosity	Surface roughness
Sample-1	74 µm	8.44gm/cm^3	2.95%	4.78 µm
Sample-2	128 µm	8.44gm/cm^3	2.85%	4.8 µm
Sample-3	215 µm	8.44gm/cm^3	2.90%	4.82 µm

2.4 Phase analysis of Stellite 6 coating

Fig. 4 shows the XRD pattern of the Stellite 6 coating. From the XRD plot, it is observed that the structure of the coating consists of a cobalt solid solution along with $Cr_{23}C_6$, Cr_7C_3, and CrO. At the highest peak intensity with a diffraction angle of 45 degrees, the carbides of Chromium ($Cr_{23}C_6$ and Cr_7C_3), coincide with the Co-based matrix. Due to instant cooling after deposition of the powder on SS 304 steel plate during the atmospheric plasma spray process, cobalt fails to undergo the alteration of equilibrium phase, thus permitting it to remain in FCC structure consistent with the temperature exceeding 417 ^{0}C. [28] There is also a small peak of CrO from the XRD pattern. The presence of CrO indicates that some oxidation of chromium might have taken place during the plasma spraying process.

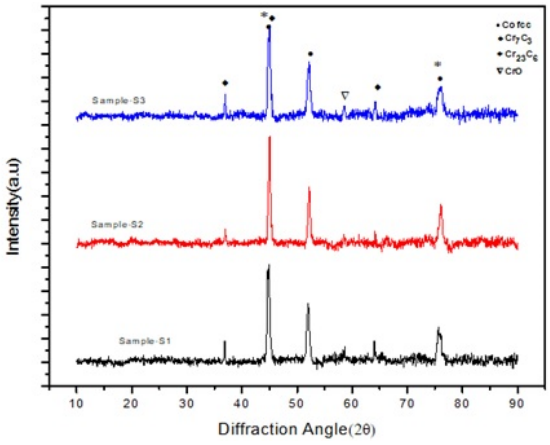

Figure 4. XRD pattern of Stellite 6 coating

2.5 Analysis of coating microstructure

Fig. 5 shows the SEM image of the plasma-sprayed Stellite 6 coating on the AISI304 substrate. It is observed that two different phases are visible from the micrograph. The light grey region corresponds to structure 1 enriched with Cobalt called a dendritic phase while the dark grey phase corresponds to structure 2 enriched with Chromium which is also called the interdendritic eutectic phase. This inter-dendritic eutectic phase consists of Cobalt with Chromium carbide [29, 30] and the dendritic phase consists of a Cobalt solid solution (FCC structure). Solid solution hardening and precipitation of carbides play a great role to provide strength to the cobalt-based superalloy.

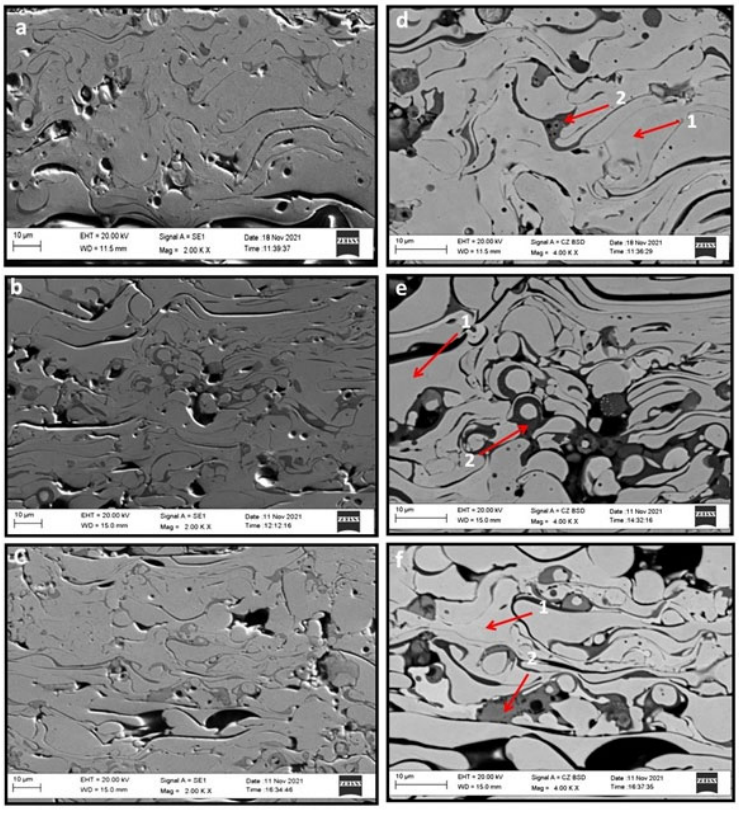

Fig. 5. SEM micrograph of Stellite 6 coatings at different magnification (a), (d) sample1, (b), (e) sample 2 and (c), (f) sample 3

It is also observed from XRD that Chromium is the main element forming carbide during the coating process. It also improves the solid solution hardening along with resistance to corrosion and oxidation. The carbides like $Cr_{23}C_6$ and Cr_7C_3

are formed by Chromium. But due to the metastable nature of Cr_7C_3 sometimes it converts into $Cr_{23}C_6$ during a higher temperature working environment.[31]

The corresponding EDS analysis of different structures (marked as 1 and 2 in the micrograph) in all the samples presented in **Fig. 6** is shown in **Table 2.** From this table, it is found that Co, Cr, and W are the dominant elements in the dendritic as well as the inter-dendritic region. Oxygen is present in the inter-dendritic region in an abundant manner mostly due to SiO_2. Some oxides of Cr appear as thin dark (black) phases and are located as a marginal line between the laminas. These are formed instantly after the deposition process due to the reaction of lamellae with the adjacent air.[32,33] When W and Mo are present in the microstructure of Stellite 6 they provide strength by forming carbides or intermetallic compounds. [30, 32] But the presence of W from EDS elemental mapping analysis is very less as compared with Co and Cr. So, there is no presence of the white phase which is enriched with tungsten as seen from PTA-coated surfaces.[28, 34] Hence it is assumed that tungsten is embedded in the cobalt matrix within the inter-dendritic phase and provides additional strength employing solid solution hardening.

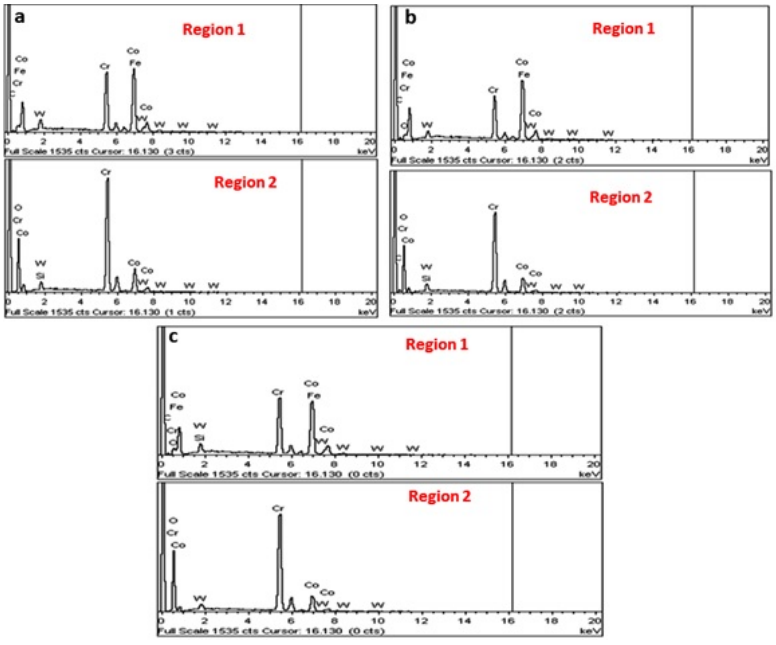

Fig. 6. EDS analysis of different structures in (a) Sample1 (b) Sample 2 (c) Sample 3

Table 2. EDS analysis of Stellite 6 coatings

Samples	The marked region in the micrograph	Co	Cr	W	Fe	C	O	Si
Sample 1	1	56.71	29.64	6.58	2.32	4.75	---	---
	2	21.02	57.02	2.16	----	---	18.53	1.27
Sample 2	1	62.74	23.07	5.48	1.91	6.18	0.61	---
	2	16.26	51.54	2.21	---	6.09	22.45	1.45
Sample 3	1	57.29	30.82	3.89	1.35	4.94	0.3	1.4
	2	16.45	57.11	3.36	---		23.08	---

2.6 Analysis of microhardness

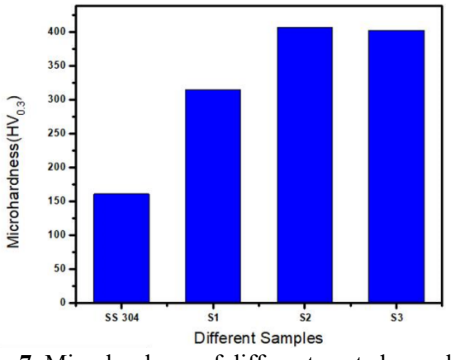

Fig. 7. Microhardness of different coated samples

Fig. 7 shows the microhardness values of the coated materials undertaken on the SS 304 substrate. The average microhardness value of the uncoated substrate has increased from 161 ± 2 $HV_{0.3}$ to 375 ± 42.5 $HV_{0.3}$ (Stellite 6 coated samples). The observed increase in microhardness in the coated samples may be due to the consistent dispersal of carbides in the Stellite 6 matrix and also due to grain refinement, and uniform and regular grain size. Sample1 exhibits the lowest hardness of 315 $HV_{0.3}$ as compared to the other samples. The Microhardness of sample 2 & sample 3 is nearly identical. As the coating thickness of the sample is very small so it gets punctured thus reflecting the hardness of the substrate. The hardness value of (402.6 ± 20.9 HV $_{(2.94\ N)}$) was obtained for the Stellite6 materials produced through sand casting and reported by Yu et al.[35]

2.7 Electrochemical corrosion

Three Stellite 6 coated samples having different coating thicknesses deposited on SS-304 steel substrate had undergone electrochemical potentiodynamic corrosion test to check the corrosion resistant property. The polarization curves of all specimens along with SS 304 are shown in **Fig. 8** and the corrosion rate of all samples was measured and summarized in **Table 3.** In the test solution, the corrosion potential and corrosion current density are the evaluating parameters of measurement of the intensity of corrosion. Coated samples with less corrosion current density and higher corrosion potential value indicate superior corrosion resistance characteristics. [20, 24, 36] From the results obtained through the electrochemical corrosion test it was inferred that a sample coated with 215 microns (S3) coating thickness exhibits the lowest corrosion current density and highest corrosion potential. Moreover, it has the lowest corrosion rate showing the best corrosion-resistant properties as compared to other coated samples. The presence of higher Chromium content in Stellite 6 alloys enhances higher oxidation and corrosion resistance properties by forming a protective Cr_2O_3 film which is observed in the polarization curves.

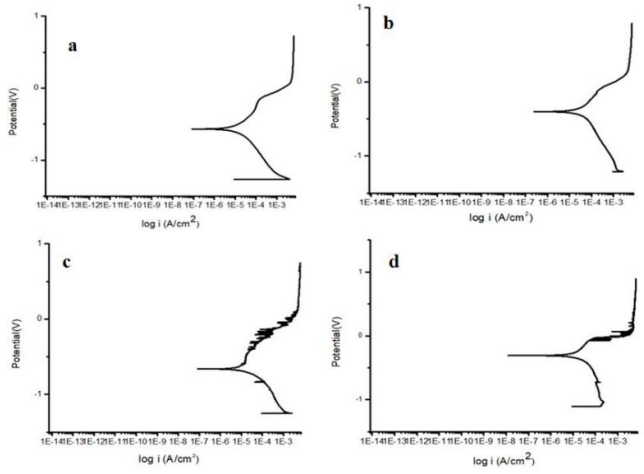

Fig. 8. Potentiodynamic polarization curves of (a) SS 304, (b) Specimen1, (c) Specimen 2, (d) Specimen 3

Table 3. Electrochemical parameters determined through potentiodynamic corrosion test

Specimens	E-corrosion(V)	J-corrosion(A/Cm^2)	Corrosion rate(mm/year)
SS-304	-0.5677	1.2567×10^{-5}	0.14603
S1	-0.40104	9.9162×10^{-6}	0.11523
S2	-0.66121	5.2194×10^{-6}	0.060649
S3	-0.30757	4.0335×10^{-6}	0.046869

Corrosion is a type of surface phenomenon in which the manifestation of failure starts from the outer surface and gradually progresses toward the inner core (substrate). Sample 3 possesses the presence of three layers of Stellite 6 coating on a SS 304 stainless steel substrate retards the onset of the corrosion process. Progress of corrosion takes much more time to reach the SS 304 surface and provides the best corrosion-resistant property as compared to the other two coated samples. It can be seen from Figure 8(a), (b) that Stainless Steel 304 substrate and sample 1 have identical corrosion resistance properties and likely succumb to corrosion. Similarly, from Figure 8(c), sample 2 with higher coating thickness gives better resistance to corrosion and the time required for undergoing corrosion is also enhanced compared to the first sample. In Figure 8(d), sample 3 with 215-micron coating thickness provides superior resistance to undergo the process of corrosion. Because of the coating, the corrosion resistance has increased by 68.4 percent. A phenomenon of acceleration and retardation of corrosion initiation is visible clearly in the Tafel plot but ultimately succumbs to corrosion after a longer interval of time as compared to the other two samples.

3. Conclusions

Stellite 6 powder was successfully deposited on AISI 304 stainless steel substrate by atmospheric plasma spray process without any intermittent bond coat. Three stainless steel rolled plate samples were coated on a flat surface having 74 microns in a single layer, 128 microns on the double layer and 215-micron coating thickness was obtained for three layers of coatings. Coated surface was smooth, homogeneous, and free from any defects for higher coating thickness as indicated by scanning electron microphotographs. The adhesion strength between the substrate and coating was obtained between 26.5±2 MPa indicating a uniform strength for coated products. Sample coated with Stellite 6 powder having 128-micron (sample 2) coating thickness is exhibiting the best microstructure and mechanical properties, whereas sample 3 having 215-micron coating thickness exhibits better corrosion-resistant properties as compared to the other two coated samples. This can be concluded that Stellite 6 coated on Stainless steel plate may have superior mechanical properties but is having a marginal improvement for corrosion resistant properties. An improvement of 68.4 percent was evinced for corrosion resistance property in sample 3 with 215-micron coating thickness. Thus, a judicious approach of optimization is necessary for selecting the coating thickness depending on its application.

Acknowledgments

The authors are grateful to the Director, CSIR-Institute of Minerals and Materials Technology (CSIR-IMMT), Bhubaneswar for providing necessary support for conducting the experimental work.

4. Materials and Experimental details

4.1 Substrate Material

Austenitic grade AISI 304 Stainless Steel was procured from Jindal Stainless, a world leader in manufacturing stainless steel plates. This grade of steel is widely used in industry as structural steel. Three test samples rolled from a 3 mm stainless steel plate having dimensions of 100mm x 60mm were identified as the substrate material for coating and conducting experiments. The chemical composition of the substrate material in wt% is shown in Table 4. Commercially available AISI 304 Stainless Steel plate obtained from the rolling mills has a surface finish of either 1 µm or 3 µm. Before undertaking the coating procedure, surface preparation of the substrate material was conducted to improve the bond strength between the substrate and coating material. The cleaning was done before the grit blasting using ethanol and an ultrasonic cleaner. Subsequently grit blasting of alumina with a grit size of 400 µm on AISI 304 Stainless Steel substrate was done to enhance the surface roughness in the range of 4-5 µm that ameliorates mechanical interlocking between the substrate and coating before depositing the coated material through plasma spraying technique.

4.2 Coating Powder

Cobalt-based Stellite 6 powder (M/S. Metallizing Equipment Co. Pvt. Ltd., Jodhpur, India) was used as a coating material on AISI 304 Stainless Steel substrate. The particle size distribution of the powder was measured using a particle size analyzer by adopting a laser diffraction technique. It was observed that the nominal particle size distribution of the powder was between 15 µm to 45µm. The chemical composition of the supplied Stellite 6 powder was determined using an Optical Emission Spectrometer (OES) and the findings are shown in Table 4. The Stellite 6 powder is used as the feedstock powder for coating the steel substrate through the atmospheric plasma spraying process.

Table 4. Chemical composition of AISI 304 stainless steel and Stellite 6 powder

AISI 304		Stellite 6	
Element	**Wt.%**	**Element**	**Wt.%**
Cr	18.736	Co	57.822
Ni	8.288	Cr	32.273
Si	0.366	W	4.7909
Mn	1.440	Ni	2.4611
C	0.023	Fe	1.1275
S	0.006	Mo	0.2956
P	0.029	C	0.98
Fe	Balance	Si	0.95
		Mn	0.2281
		Nb	0.005

4.3 Plasma Process Parameters

Plasma spray torch PS-50 (Make Metallisation, UK), a non-transferred type consisting of an 8mm nozzle diameter with 80KW maximum capacity was used for the deposition of the coating particles. The Stellite 6 powder as feedstock material was injected into the plasma jet produced using argon and hydrogen gases. The carrier gas (Ar) transports the powder from the powder feeder unit to the plasma plume which also inhibits oxidation. After the grit blasting, the plasma coating was carried out directly. The process parameters for the plasma spraying process are listed in **Table 5**. The parameters used in

the spraying process are kept constant throughout the experiment. The deposition efficiency of the process was 45%. It is calculated from the fact that the total powder is thrown towards the substrate concerning the mass gain of the substrate. The coating on the substrate is done using a robot with application software. The coating is accomplished by depositing the powder layer by layer on the steel substrate by longitudinal and transverse deposition adopting weaving technique alternately as shown in **Fig. 9**. The powder feeding rate was always kept to 8gm/min. The substrate always remains stationary, and the torch was moving at a speed of 2m/sec. During the complete deposition process, it was ensured that the temperature of the substrate never goes beyond 120^0 C. The total number of torches passes gradually increased and accordingly, the total deposition time also increased producing increased thickness of the coated sample.

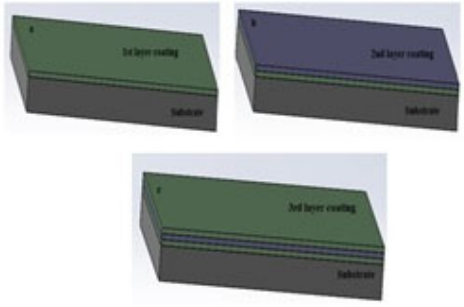

Fig. 9. Methodology of deposition, (a) Sample 1, (b) Sample 2, (c) Sample 3

Table 5. Plasma spray process parameter for spraying Stellite 6 powder

Parameters	Value
Current(A)	500
Voltage (V)	43.1
Power (Kw)	21.4
Primary gas(Ar) flow rate(l/min)	40
Secondary gas (H_2) flow rate(l/min)	0.2
Carrier gas (Ar) flow rate(l/min)	5
Primary feeder plate(RPM)	4
Nozzle to substrate distance (mm)	110
Preheating details	No preheating

4.4 Characterization of Coating

Different phases present in the powder and the coatings were investigated using an X-ray Diffractometer instrument with CuKα (λ = 1.5406 Å) 40 mA by adopting the JCPDS database card. The scanning angle range was varied from 10° to 80°, by a step width of 0.02 and a time of 5s per step. The surface morphology of powder and coating were analyzed using a scanning electron microscope (EVO MA 10, CARL ZEISS, Germany), equipped with Energy Dispersive X-ray Spectroscopy (EDS) for elemental analysis at different phases. By using a diamond wheel cutter the samples were cut and mounted in resin using a hot mounting press for the inspection of the cross-section of the coating. The mounted samples were polished with emery paper with a different grit size of SiC and got the final mirror polish shape by using diamond paste. Then the samples were cleaned with distilled water, cloth polished, and dried properly to reveal the microstructure using optical microscopy and SEM.

The density of the coating was determined by peeling a small portion from the surface of the substrate and using the Archimedes principle to know the homogeneity of the deposition. Surface roughness and adhesion tests were performed to know the roughness of the coating surface and the bond strength of the coating with the substrate respectively. The adhesion strength of the 100 mm x 60 mm sample size was carried out with a stud pull automatic adhesion tester (S/N AT12983, Defelsko positest AT-A, USA). The aluminum stud of 10 mm diameter has mounted on the surface of the coated sample by making the use of an epoxy paste (HTK ultra-bond 100) after proper surface cleaning with emery and acetone. Assembled system is then put into an oven at 150˚C for 80 minutes for the curing of the epoxy paste. Two specimens of each sample were produced for testing the adhesion strength and the average value with standard deviation is considered. The microhardness of the coating measurement was tested using a Vickers microhardness tester (VH3300, BUEHLER, USA). A load of 300g was maintained throughout the experiments for a time duration of 10s. An average or mean value of five indentations on the cross-sectional interface of the coating is considered.

4.5 Corrosion resistance test

Potentiodynamic electrochemical corrosion tests on the specimens with various coating thicknesses were carried out in 3.5 weight percent sodium chloride (NaCl) solution using Autolab PGSTAT302N potentiostat measurement system. The functional behavior of the coating such as corrosion was conducted according to ASTM: G 59 -97 (2003) standard. It is one of the common corrosion testing methods conducted to ascertain the corrosion resistance characteristics of different types

of metals. A saturated silver-silver chloride calomel electrode (SCE) was used as the reference electrode and the auxiliary electrode was made of platinum. Test specimen of 10 mm square was immersed in the test solution for 30 minutes before the commencement of corrosion tests. The potential range was set between -1 mV to 1 mV with a scan rate of 0.5 mV/s. The readings obtained from experiments were recorded and subsequently examined with NOVA 2.1.3 application software for the interpretation of test results.

References

1 Hidalgo V. H., Varela J. B., Menéndez A. C., and Martınez, S. P. (**2001**) High temperature erosion wear of flame and plasma-sprayed nickel–chromium coatings under simulated coal-fired boiler atmospheres. *Wear*, *247*(2), 214-222.

2 Ahmed R., Elameen M., Faisal N. H., El-Sherik A. M., Elakwah Y. O., and Goosen, M. F. A. (**2014**) Single asperity nano scratch behavior of HIPed and cast Stellite 6 alloys. *Wear*, 312 (1-2) 70-82.

3 Apay S., and Gulenc, B. (**2014**) Wear properties of AISI 1015 steel coated with Stellite 6 by microlaser welding. *Mater. Des.*, *55,* 1-8.

4 Giacchi J. V., Morando C. N., Fornaro O., and Palacio, H. A. (**2011**) Microstructural characterization of as-cast biocompatible Co–Cr–Mo alloys. *Mater. Charact.*, *62*(1) 53-61.

5 Pawlowski L. (**2008**) *The science and engineering of thermal spray coatings*. John Wiley & Sons.

6 Di Girolamo G., Brentari A., Blasi C., and Serra E. (**2014**) Microstructure and mechanical properties of plasma sprayed alumina-based coatings. *Ceram. Int.*, *40*(8), 12861-12867.

7 Zavareh M. A., Sarhan A. A. D. M., Abd Razak B. B., and Basirun W. J. (**2014**) Plasma thermal spray of ceramic oxide coating on carbon steel with enhanced wear and corrosion resistance for oil and gas applications. *Ceram. Int.*, *40*(9), 14267-14277.

8 Toma D., Brandl W., and Marginean, G. (**2001**) Wear and corrosion behaviour of thermally sprayed cermet coatings. *Surf. Coat. Technol.*, *138*(2-3), 149-158.

9 Liao H., Normand B., and Coddet C. (**2000**) Influence of coating microstructure on the abrasive wear resistance of WC/Co cermet coatings. *Surf. Coat. Technol.*, *124*(2-3), 235-242.

10 Swain B., Mallick P., Bhuyan S. K., Mohapatra S. S., Mishra S. C., and Behera, A. (**2020**) Mechanical properties of NiTi plasma spray coating. *J. Therm. Spray Technol.*, *29*(4), 741-755.

11 Zhang P. X., Yan, H., and Sun, Y. H. (**2021**) Microstructure, microhardness and corrosion resistance of laser cladding Al2O3@ Ni composite coating on 304 stainless steel. *J. Mater. Sci.*, *56*(13), 8209-8224.

12 Zhai L. L., Ban C. Y., and Zhang J. W. (**2019**) Microstructure, microhardness and corrosion resistance of NiCrBSi coatings under electromagnetic field auxiliary laser cladding. *Surf. Coat. Technol.*, *358*, 531-538.

13 Luo F., Cockburn A., Lupoi R., Sparkes M., and O'Neill, W. (**2012**) Performance comparison of Stellite 6® deposited on steel using supersonic laser deposition and laser cladding. *Surf. Coat. Technol.*, *212,* 119-127.

14 Lin W. C., and Chen C. (**2006**) Characteristics of thin surface layers of cobalt-based alloys deposited by laser cladding. *Surf. Coat. Technol.*, *200*(14-15), 4557-4563.

15 Budzyński P., Kamiński M., Turek M., and Wiertel M. (**2020**) Impact of nitrogen and manganese ion implantation on the tribological properties of Stellite 6 alloy. *Wear*, *456*, 203360.

16 Thawari N., Gullipalli C., Katiyar J. K., and Gupta T. V. K. (**2021**) Influence of buffer layer on surface and tribomechanical properties of laser cladded Stellite 6. *Mater. Sci. Eng. B Solid State Mater.Adv.Technol.*, *263*, 114799.

17 Jeyaprakash N., Yang C. H., and Tseng S. P. (**2021**) Wear Tribo-performances of laser cladding Colmonoy-6 and Stellite-6 Micron layers on stainless steel 304 using Yb: YAG disk laser. *Met. Mater. Int.*, *27*(6), 1540-1553.

18 Magarò P., Marino A. L., Di Schino, A., Furgiuele F., Maletta C., Pileggi R., Sgambitterra E., and Tului M. (**2019**) Effect of process parameters on the properties of Stellite-6 coatings deposited by Cold Gas Dynamic Spray. *Surf. Coat. Technol.*, *377*, 124934.

19 Sassatelli P., Bolelli G., Gualtieri M. L., Heinonen E., Honkanen M., Lusvarghi L., Manfredini T., Rigon R., and Vippola, M. (**2018**) Properties of HVOF-sprayed Stellite-6 coatings. *Surf. Coat. Technol.*, 338 45-62.

20 Bartkowski D., Młynarczak A., Piasecki A., Dudziak B., Gościański M., and Bartkowska, A. (**2015**) Microstructure, microhardness and corrosion resistance of Stellite-6 coatings reinforced with WC particles using laser cladding. *Opt. Laser Technol.*, *68*, 191-201.

21 Dinega D. P., and Bawendi M. G. (**1999**) A solution-phase chemical approach to a new crystal structure of cobalt. *Angew. Chem. Int. Ed.*, *38*(12) 1788-1791.

22 Duflos F., & Stohr J. F. (**1982**) Comparison of the quench rates attained in gas-atomized powders and melt-spun ribbons of Co-and Ni-base superalloys: influence on resulting microstructures. *J. Mater. Sci.*, *17*(12) 3641-3652.

23 Biswal S. R.,and Sahoo S. (**2020**) Fabrication of WS2 Dispersed Al-Based Hybrid Composites Processed by Powder Metallurgy: Effect of Compaction Pressure and Sintering Temperature. *J. Inorg. Organomet. Polym. Mater.*, *30*(8) 2971-2978.

24 Stellite Alloys-Chemical composition, Mechanical Properties Retrived from:https://www.azom.com/article.aspx?ArticleID=9857

25 Debasish D., Bajpai S., Gochhayat S., Dash T., Pati A. R., Patra P. K., Bhagat A. N., Singh S.K., and Rout T. K. (**2022**) Plasma processing of Fe-P/rGO powder for making robust wear resistance and anticorrosion coating over mild steel. *Mater. Res. Express.*, *9*(2) 026526.

26 Sidhu B. S., and Prakash S. (**2006**) Studies on the behaviour of stellite-6 as plasma sprayed and laser remelted coatings in molten salt environment at 900 C under cyclic conditions. *J. Mater. Process. Technol.*, *172*(1) 52-63.
27 Sidhu H. S., Sidhu B. S., and Prakash, S. (**2007**) Solid particle erosion of HVOF sprayed NiCr and Stellite-6 coatings. *Surf. Coat. Technol.*, *202*(2) 232-238.
28 Men X., Tao F., Gan L., Zhao F., and Xu Z. (**2019**) Erosion behavior and surface cracking mechanism of Co-based coating deposited via PTA under high-speed propellant airflow. *Surf. Coat. Technol.*, *372*, 369-375.
29 Lolla T., Siefert J., Babu S. S., and Gandy D. (**2014**) Delamination failures of Stellite hardfacing in power plants: a microstructural characterisation study. *Sci. Technol. Weld. Join.*, *19*(6), 476-486.
30 Singh R., Kumar D., Mishra S. K., and Tiwari, S. K. (**2014**) Laser cladding of Stellite 6 on stainless steel to enhance solid particle erosion and cavitation resistance. *Surf. Coat. Technol.*, *251*, 87-97.
31 Davis, J. R. (**2000**) Nickel, cobalt, and their alloys. ASM international.
32 Deshpande S., Sampath S., and Zhang H. (**2006**) Mechanisms of oxidation and its role in microstructural evolution of metallic thermal spray coatings—Case study for Ni–Al. . *Surf. Coat. Technol.*, *200*(18-19), 5395-5406.
33 Dent A. H., Horlock A. J., McCartney D. G., and Harris S. J. (**2001**) Microstructural characterization of a Ni-Cr-BC based alloy coating produced by high velocity oxy-fuel thermal spraying. . *Surf. Coat. Technol.*, *139*(2-3), 244-250.
34 Sawant M. S., and Jain N. K. (**2017**) Investigations on wear characteristics of Stellite coating by micro-plasma transferred arc powder deposition process. *Wear*, *378*, 155-164.
35 Yu H., Ahmed R., Lovelock H. D. V., and Davies S. (**2009**) Influence of manufacturing process and alloying element content on the tribomechanical properties of cobalt-based alloys, *J. Tribol.*, *131*(1), 011601.
36 Liu R., Yao J., Zhang Q., Yao M. X., and Collier R. (**2015**) Effects of molybdenum content on the wear/erosion and corrosion performance of low-carbon Stellite alloys. *Mater. Des.*, *78*, 95-106.